## Title

Toward a unified connectomic target for deep brain stimulation in obsessive-compulsive disorder

## Authors

Ningfei Li[1]*, Juan Carlos Baldermann[2], Astrid Kibleur[3,4], Svenja Treu[5], Harith Akram[6,7], Gavin J.B. Elias[8], Alexandre Boutet[8,9], Andres M. Lozano[8], Ludvic Zrinzo[6,7], Eileen Joyce[6,7], Stephan Chabardes[3], Veerle Visser-Vandewalle[10], Mircea Polosan[3,11,12], Jens Kuhn[2,13], Andrea A. Kühn[1], Andreas Horn[1]

1. Movement Disorders & Neuromodulation Unit, Department for Neurology, Charité University Medicine Berlin, Germany.
2. Department of Psychiatry and Psychotherapy, University of Cologne, Medical faculty, Cologne, Germany.
3. Univ. Grenoble Alpes, F-38000 Grenoble, France.
4. OpenMind Innovation, F-75008 Paris, France.
5. Laboratory for Clinical Neuroscience, Centre for Biomedical Technology, Universidad Politecnica de Madrid, Spain.
6. Department of Clinical and Movement Neurosciences, UCL Queen Square Institute of Neurology, London, UK.
7. National Hospital for Neurology and Neurosurgery, UCL Queen Square Institute of Neurology, London, UK.
8. University Health Network, Toronto, Ontario, Canada.
9. Joint Department of Medical Imaging, University of Toronto, Ontario, Canada
10. Department of Stereotactic and Functional Neurosurgery, University of Cologne, Cologne, Germany.
11. Inserm, U1216, Grenoble Institut des Neurosciences, F-38000 Grenoble, France.
12. Psychiatry Department, CHU Grenoble Alpes, F-38000 Grenoble, France.
13. Johanniter Hospital Oberhausen, EVKLN, Department of Psychiatry, Psychotherapy and Psychosomatics, Oberhausen, Germany.

* **Corresponding Author**

Ningfei Li
Department of Neurology, Movement Disorders and Neuromodulation Unit, Charité - University Medicine (CCM), Berlin, Germany.
E-mail: ningfei.li@charite.de

## Abstract

Multiple surgical targets have been proposed for treating obsessive-compulsive disorder (OCD) with deep brain stimulation (DBS). However, different targets may modulate the same neural network responsible for clinical improvement. Here we analyzed data from two cohorts of OCD patients that underwent DBS to either the anterior limb of the internal capsule (ALIC) or the subthalamic nucleus (STN). Fiber tracts that were predominantly connected to electrodes in good or poor DBS responders – based on improvement on the Yale-Brown Obsessive-Compulsive Scale (Y-BOCS) – were isolated and each assigned a predictive value. Strikingly, the same fiber bundle that was positively discriminative of treatment response emerged in both cohorts, independently from each other. Using this tract, it was feasible to cross-predict clinical improvement across DBS targets, cohorts and centers. Finally, the clinical outcome of six additional patients from a third center with electrodes implanted in both targets was predicted based on this novel tract-based DBS target. Main results were replicated based on a pathway atlas of the basal ganglia. Our results suggest a functional role of cortical input from dorsal anterior cingulate cortex and ventrolateral prefrontal cortex to the STN. Furthermore, obsessive-compulsive symptoms could indeed be modulated by stimulation of a specific bundle that is now well-represented in three-dimensions. Finally, we show that connectivity-derived improvement models that are informed by patients operated in one target can predict outcome in patients operated in an alternative target, and vice versa.

Obsessive-compulsive disorder is a debilitating disease with a life-time prevalence of around 2.3% [1]. Treatment of severe cases by deep brain stimulation (DBS) to the anterior limb of the internal capsule has been approved by the FDA (Humanitarian Device Exemption) in 2009. A variety of other targets have been proposed, however, including the STN [2,3], ALIC [4], nucleus accumbens (NAc) [5–7], ventral capsule/ventral striatum (VC/VS) [8], inferior thalamic peduncle (ITP) [9,10], bed nucleus of the stria terminalis (BNST) [11], anteromedial globus pallidus interna (amGPi) [12], superolateral branch of the medial forebrain bundle (slMFB) [13] and medial dorsal and ventral anterior nucleus of the thalamus (MD/V ANT) [14] (for an overview of targets see [15]). A recent prospective clinical trial implanted four electrodes per patient with one pair in the STN and one in the ALIC [16].

In parallel, DBS has experienced a conceptual paradigm-shift away from focal stimulation of specific brain nuclei (such as the subthalamic nucleus or globus pallidus in Parkinson's Disease; PD) toward modulating distributed brain networks (such as the motor basal-ganglia cortical cerebellar loop in PD) [17–19].

Thus, it could be possible that, of the multiple targets proposed, some or most may in fact modulate the same brain network to alleviate symptoms. Such a concept has been proposed in the past by Schlaepfer and colleagues for the case of treatment-refractory depression [20]. According to their concept, the supero-lateral branch of the medial forebrain bundle may connect most if not all surgical targets that were proposed for treatment of depression (e.g. subgenual cortex, ALIC, NAc, habenula). In a recent study, it was further implied that smaller distances to the slMFB were associated with better clinical improvement in OCD patients implanted for ventral ALIC-DBS, even though the anatomical position of the electrodes themselves were not related to treatment response [21]. Thus, in theory, the *tract itself* could be a surgical target – and could be modulated in a similar way when targeting various points along its anatomical course. Accordingly, already, Coenen and colleagues surgically implanted electrodes in two OCD patients, targeting a tract instead of a localized target [13]. The tract connected the ventral tegmental area and the prefrontal cortex and authors referred to it as the superolateral branch of the medial forebrain bundle.

Other invasive therapies, such as cingulotomy and capsulotomy primarily aimed at disrupting connectivity to frontal regions by lesioning white matter bundles [22]. Moreover, it was recently shown that such tract- or network-based concepts could be used to predict clinical improvement across DBS centers and surgeons for the case of Parkinson's Disease [18]. Using modern neuroimaging methods and high-resolution connectomic datasets, it could be shown that connectivity of the DBS electrodes to specific cortical regions is associated

with stronger therapeutic effects in various diseases treated with the surgical procedure [18,23–26].

For the case of OCD, Baldermann and colleagues have recently demonstrated that structural connectivity from DBS electrodes to medial and lateral prefrontal cortices were associated with stronger symptom alleviation [23]. Crucially, they were also able to identify a specific subsection of the ALIC that was highly associated with symptom improvement after one year of DBS. Of note, connectivity to this fiber tract was able to predict ~40 % of the variance in clinical outcome of this sample. Already in their study, the bundle was described to connect to both the medial dorsal nucleus of the thalamus (which has received substantial attention in the context of OCD) and to the anterior part of the STN. The STN itself is a prominent target for DBS of various diseases including PD [27], dystonia [28], OCD [29] and Tourette's Syndrome [30]. The small nucleus receives wide-spread direct afferents from most parts of the prefrontal cortex and is involved in motor, associative and limbic processing [31]. Likely due to these cortico-subthalamic projections, the nucleus has various functional zones that largely follow the organization of the frontal cortex, i.e. the sensorimotor parts of the STN are posterior and followed by pre-/oculomotor-, associative and limbic domains in anteromedial direction.

Consequently, the anterior (associative/limbic) parts of the STN have been targeted by DBS for OCD [29]; these same subregions were also exclusively connected to the tract-target identified by Baldermann and colleagues in ALIC-DBS patients [23]. Following up on this, our study aimed at testing whether the same tract may be associated with good clinical outcome in a cohort treated with STN-DBS. Thus, here, we retrospectively analyzed two cohorts of DBS patients that were treated with either STN-DBS or ALIC-DBS in order to test our hypothesis, that the same tract could potentially predict clinical improvement in STN-DBS as well as ALIC-DBS. We identify a common tract that already becomes apparent when analyzing each cohort alone. We then test predictive utility of this tract in an additional cohort of six patients from a third center. In this cohort, patients received four DBS electrodes, one pair targeting bilateral STN, the other ALIC [16].

## Results

Two cohorts (Cologne; ALIC target; N = 22; and Grenoble; STN target; N = 14) formed a training and cross-validation cohort on which the tract target was identified. Each of the two cohorts were first analyzed independently, then to cross-predict outcome in the patients from the other one. The main part of the analyses focuses on these two cohorts. Only as a final validation step, an additional test-cohort was included (London; four electrodes targeting both ALIC and STN).

Patients in both training cohorts (Cologne, Grenoble) were of similar age with a similar Y-BOCS score at baseline (see Table 1 for demographic details). Y-BOCS improvement was also comparable across groups (9.6 ± 6.5 points or 31.0 ± 20.5 % in the ALIC cohort vs. 13.8 ± 10.8 points or 41.2 ± 31.7 % in the STN cohort).

In the test cohort (London; ALIC and STN target; N = 6), stimulation parameters resulted from an optimized phase following parameter optimization. Patients improved by 21.8 ± 5.7 points (or 50.0 ± 12.6 %) on the Y-BOCS scale. Key demographic values are reported in Table 1.

**Table 1:** Patient demographic details and clinical results of the two cohorts

| | ALIC **DBS Cohort (Mean ± SD)** | STN **DBS Cohort (Mean ± SD)** | Combined **DBS Cohort (Mean ± SD)** |
|---|---|---|---|
| **Center** | **University Hospital Cologne** | **University Hospital Grenoble** | **University Hospital London** |
| Reference(s) | (22, 31) | (28) | (16) |
| N (females) | 22 (12) | 14 (9) | 6 (1) |
| Age | 41.7 ± 20.5 | 41 ± 9 | 45.5 ± 10.5 |
| Y-BOCS Baseline | 31.3 ± 4.4 | 33.4 ± 3.7 | 36.2 ± 1.8 |
| Y-BOCS after DBS | 20.7 ± 7.7 *(12 months postop)* | 19.6 ± 10.6 *(12 months postop)* | 14.3 ± 4.1 *(optimized phase in [16])* |
| Absolute Y-BOCS Improvement | 9.6 ± 6.5 | 13.8 ± 10.8 | 21.83 ± 5.7 |
| % Y-BOCS Improvement | 31.0 ± 20.5 % | 41.2 ± 31.7 % | 50.0 ± 12.6 % |

Electrode localization confirmed accurate placement to each of the two target regions for all patients from Grenoble and Cologne cohorts (Figure 1). For the test cohort, accuracy of electrode placement was localized in the original study [16].

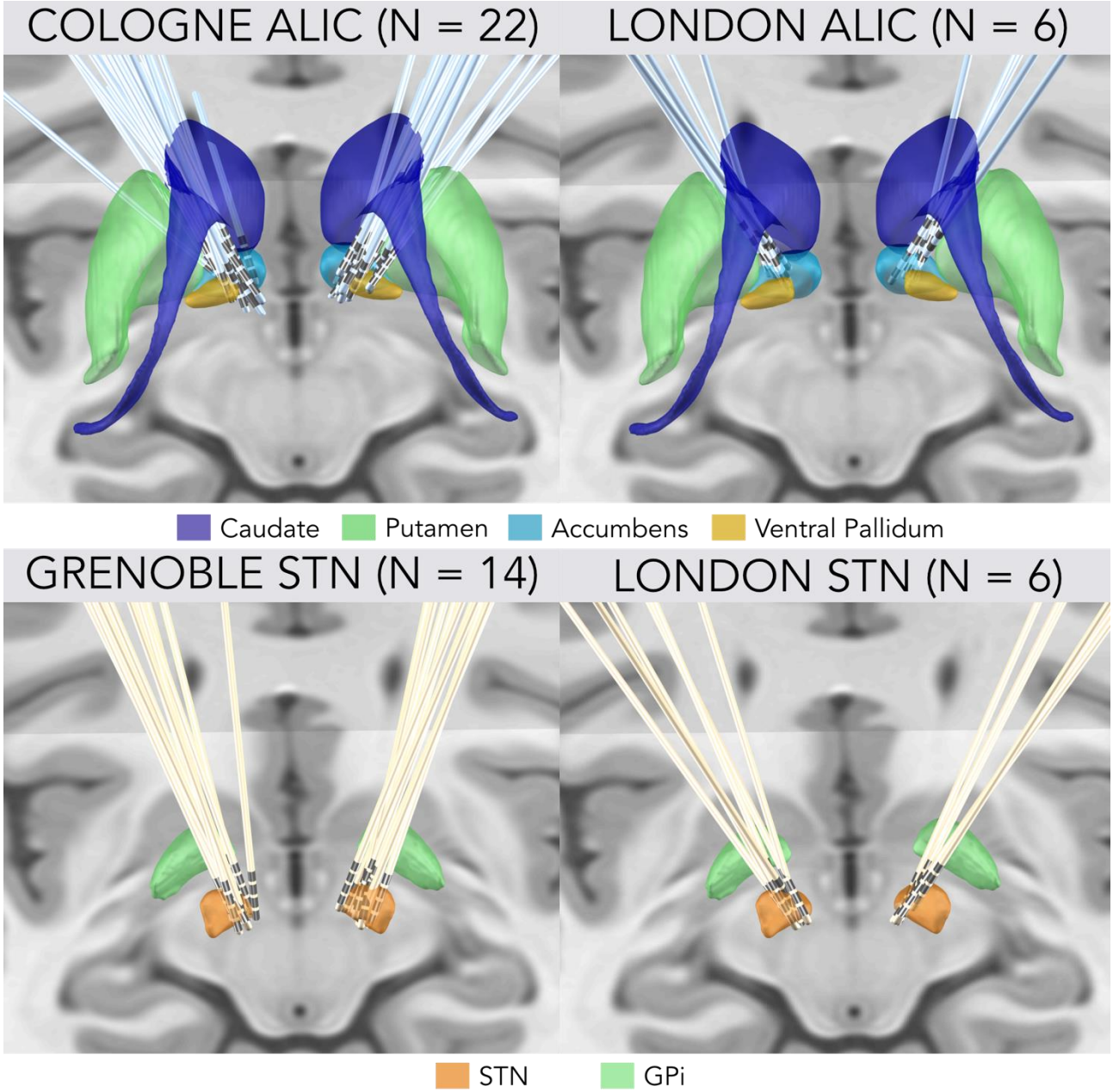


**Figure 1.** Overview of the lead electrodes placements of ALIC DBS (Cologne) and STN DBS (Grenoble) cohorts (left), as well as localizations from the test cohort with four electrodes per patient (London). Subcortical structures defined by CIT168 Reinforcement Learning Atlas [32] (ALIC cohort) and DISTAL Atlas [33] (STN cohort), with coronal and axial planes of the T1-weighted ICMB 152 2009b nonlinear template [34] as background.

Connectivity analysis results seeding from the electrodes of the two training and cross-validation cohorts (Cologne and Grenoble) based on the N = 985 HCP normative connectome are shown in Figure 2. The overall connectivity of electrodes to other areas in the brain (without weighing for clinical improvement) was strikingly different between the two cohorts (Figure 2, top row). This is hardly surprising given it mainly reflects the overall structural connectivity profiles of the two DBS targets and the STN as a widely connected

basal ganglia entry point and the ALIC as a white matter target are overall differently connected in the brain. However, when tracts were weighted by their ability to discriminate between good and poor responders (using the T-score method described below), a bilateral positively discriminative tract to the medial prefrontal cortex emerged that was shared by both cohorts (Figure 2, middle row). The degree of lead connectivity to this tract correlated with clinical improvement ($R = 0.63$ at $p < 0.001$ in the ALIC cohort and $R = 0.77$ at $p < 0.001$ in the STN cohort; Figure 2, bottom row).

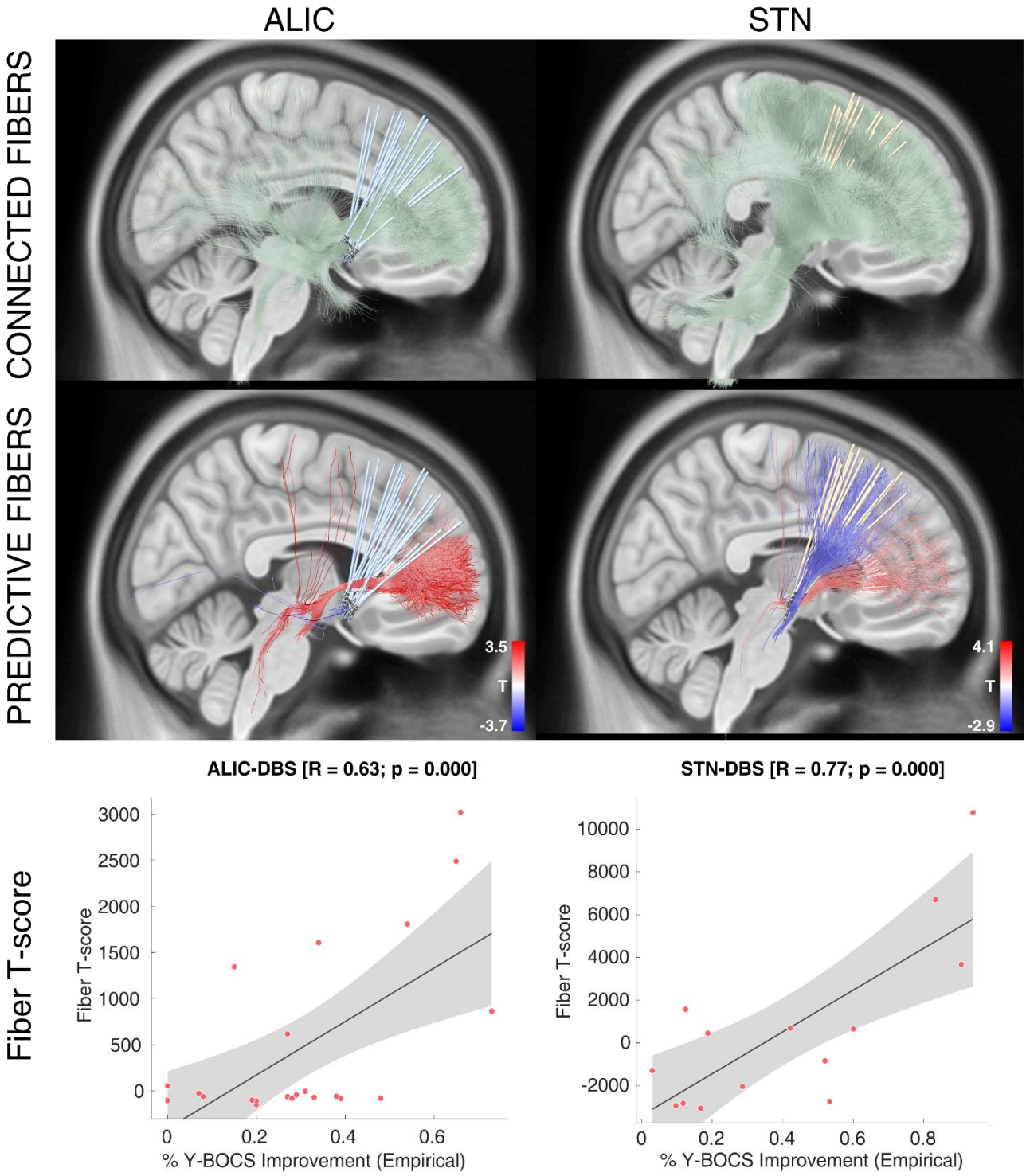


**Figure 2.** Structural connectivity of the VTA. All fibers traversing the VTA are shown in green (top row) as connected fibers. Predictive fibers positively correlated with clinical improvement are shown in red, while those negatively correlated with clinical improvement are shown in blue (mid row). The top and bottom 20% (based on Fiber T-scores) of the predictive fibers are shown. Correlations between the degree of connectivity to predictive tracts (sum of aggregated Fiber T-scores under each VTA) and the clinical improvements are shown in the bottom row. A replication of this atlas based on anatomically predefined pathways can be found in Figure S1.

Of note, these correlations are somewhat circular and meant to describe the degree of how well the tracts could explain the sample of patients on which they had been built. More interestingly, in the next step, the tract learned exclusively on the STN cohort was used to explain outcome in the ALIC cohort and vice versa (Figure 3). Here, the STN-based tract could significantly predict outcome in the ALIC cohort ($R = 0.50$ at $p = 0.009$) and vice-versa ($R = 0.49$ at $p = 0.041$).

Crucially, some VTAs of the ALIC cohort entirely resided below the identified tract and thus received a Fiber T-score of (near) zero (also see blue example patient in Figure 3, bottom right). The same holds true when either learning the tract on the STN (Figure 3) or the ALIC cohort itself (Figure 2). To further investigate this matter, two-sample t-tests between improvements of patients with near zero scores (Fiber T-scores below 50) and the remaining patients with VTAs covering the tract well (scores above 50) were calculated. This showed that electrodes that reached the tract well resulted in significantly better clinical improvement ($T = 6.5$ at $p < 10^{-5}$ when the tract was defined by the ALIC cohort and $T = 3.7$ at $p < 0.005$ when it was defined by the STN cohort).

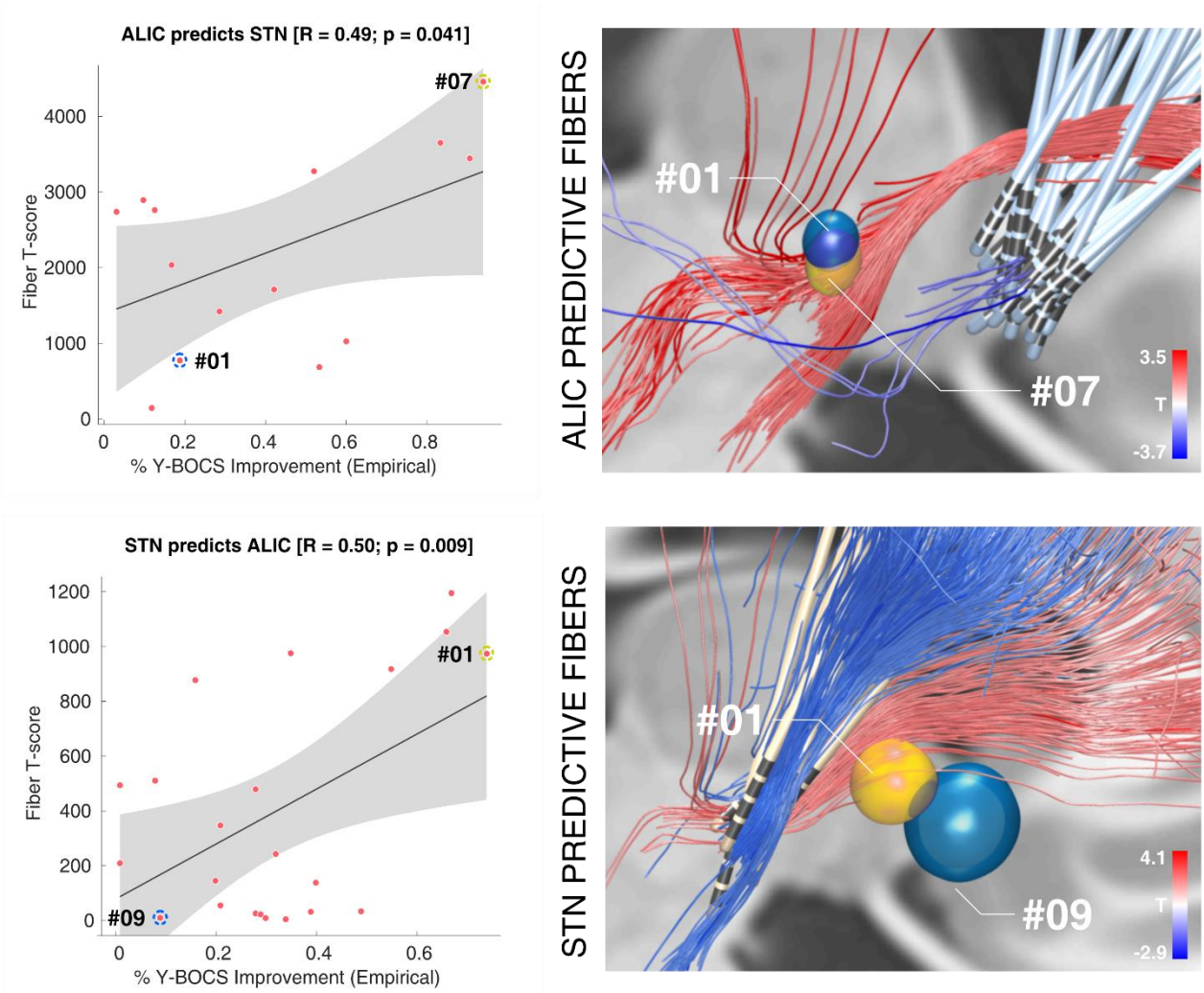

**Figure 3.** Cross-prediction between the Cologne / ALIC and Grenoble / STN cohorts. Top: The tract exclusively learned on the ALIC cohort was used to calculate Fiber T-score s for all patients in the STN cohort. One example patient with strong overlap of the tract (yellow) received a high Fiber T-score, whereas one with less overlap received a lower score (blue). The two example patients are marked in the correlation plot on the left. Bottom: Here, the tract was learned on the STN cohort to predict the ALIC patients. Again, two example patients are shown. Of note, here, some VTAs barely overlapped with the tract and consequently received a near-zero score.

In the next step, the analysis was performed on the two cohorts combined. Again, the same tract emerged even more clearly (Figure 4, left). Thus, patients with good improvement in both groups were more likely to be connected to the tract while non- or poor responders were likely not or only weakly connected to the tract. The tract passed slightly dorsal to the group of electrodes of the ALIC-cohort and coursed centrally or slightly ventral to the electrodes of the STN cohort. Depending on the target, the analysis revealed different proportions of “positive” and “negative” fibers (ALIC cohort: 22.2k positive vs. 1.9k negative fiber tracts selected from the group connectome; STN cohort: 45.1k positive vs. 48.6k negative fibers and both cohorts combined: 54.4k positive vs. 9.6k negative fibers).

The tract was then used to predict outcome in a completely independent test-set of patients that underwent surgery in a third center (London; Figure 4, right). Again, VTAs of patients that strongly overlapped fibers with positive scores and avoided tracts with negative scores received high Fiber T-scores which significantly correlated with empirical improvement, across the group ($R = 0.75$ at $p = 0.040$). Of note, VTAs in the London sample were estimated with a different software (see methods), patients received four electrodes and the clinical scores already represent an “optimized” phase following nine months of a clinical trial [16]. Still, overlap with the identified tract could successfully predict >50 % of the variance in their clinical outcome.

Given the high amount of false-positive connections present in dMRI based tractograms [35] , we replicated main findings of the study with a synthesized anatomical atlas that is purely based on established anatomical knowledge [36] and thus includes no false-positive connections. Based on this atlas, the most predictive tract was the hyperdirect pathway connecting the dorsal anterior cingulate cortex (dACC) to the STN (Figures S1-2).

The identified tract may potentially “unify” some aspects of the STN and ALIC targets for OCD. In a final analysis, we aimed at setting it into synopsis with other DBS targets that had been used in the OCD context in the literature. Using a novel method to convert stereotactic coordinates into MNI space in a probabilistic fashion [37], we converted literature-based

targets and visualized them in synopsis with the discriminative fiber tract identified in the present study (see Figure 5 and Table 2). Of note, a large number of all available DBS targets for OCD seemed to cluster on or around the anatomical trajectory of the tract identified in the present study.

This final bundle may indeed represent a “circuit-target” to treat OCD with DBS. Given its potential clinical importance, we characterized its anatomical properties using additional views relatively to anatomical landmarks (Figures 6 & S3) as well as in comparison to anatomical dissection results (Figure S4). Anatomically, the tract is a subpart of the well-characterized ALIC that connects the prefrontal cortex with the subthalamic nucleus and MD nucleus of the thalamus [38,39]. Anatomical validity of the tract was discussed with four anatomists (see acknowledgement section). In the motor domain, the “hyperdirect pathway”, i.e., a direct connection from the frontal cortex to the subthalamic nucleus, has been well established [40,41], functionally, but the STN is known to receive widespread and direct input from the prefrontal cortex as a whole [38]. Thus, the specific bundle delineated here may represent direct connectivity between frontal cortex and STN. An additional branch traversing from prefrontal cortex to the mediodorsal nucleus of the thalamus received slightly lower T-scores and is not shown in 3D visualizations but well visible in Figure 6. The main branch of the tract traverses within a specific portion of the ALIC and follows its main structural course. In the training sample (Grenoble and Cologne), the tract was slightly right-lateralized, i.e. more predictive fibers emerged on the right hemisphere and their t-scores were higher. When the same analysis was repeated on the London dataset, the same tract emerged but was even more highly right-lateralized (Figure S5). Given the small sample size of the London dataset this result should be interpreted with caution. However, studies have reported larger involvement of the right hemisphere in mediating symptom alleviation of OCD, in the past [5,23,42,43] and one study even unilaterally implanted DBS electrodes to the right ALIC [44]. However, efficacy in this study was poor and the reported evidence was based on a single case report [5].

To properly define the anatomical course of this tract, we openly released it as an atlas in stereotactic (MNI) space within Lead-DBS software (www.lead-dbs.org). Of note, Lead-DBS is scientific and not clinical software and the tract should not be used for clinical decision making [45].

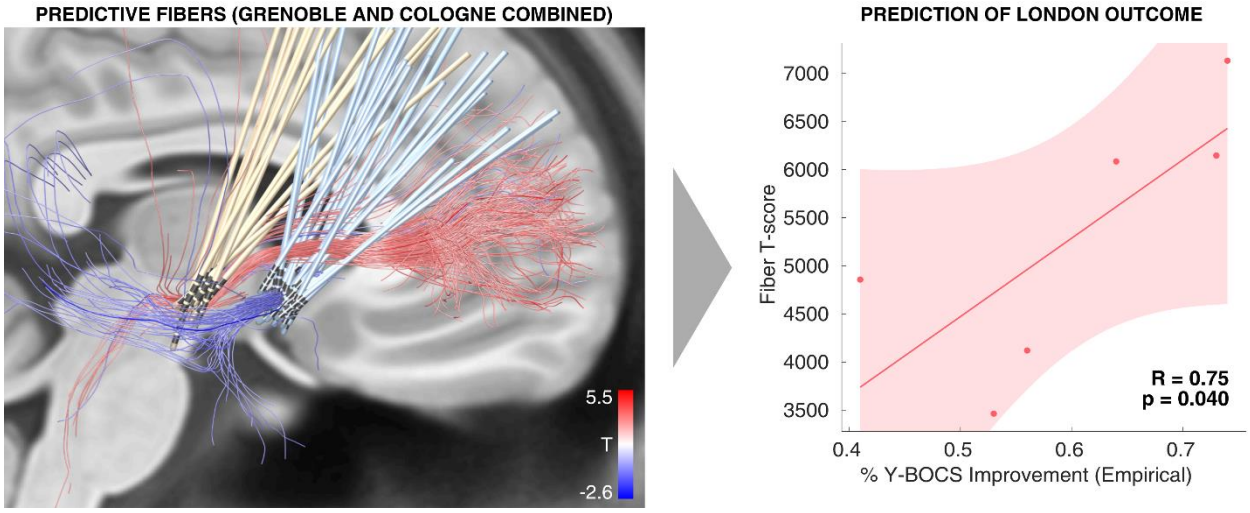


**Figure 4.** Predictive fibers when including all patients from both cohorts (Cologne, Grenoble) irrespective of their target (top). The sum of aggregated Fiber T-scores under each VTA explained % Y-BOCS improvement (bottom left). Moreover, the tract defined in one target could cross-predict improvement in the cohort treated with the other target (bottom right). Red fibers are positively associated with clinical improvement, blue fibers negatively. A replication of this atlas based on anatomically predefined pathways can be found in Figure S2.

**Table 2:** DBS targets for treatment of OCD based on literature results. *MD*, medial dorsal thalamic nucleus; *VA*, ventral anterior thalamic nucleus; *iml*, internal medullary lamina; *MCP*, mid-commissural point; *AC*, anterior commissure
* Tourette patients, with prominent symptoms of OCD

| DBS Target | Reference | Number of patients | % YBOCS change | AC/PC coordinates | Relative to | Target type | MNI coordinates (Figure 5) |
|---|---|---|---|---|---|---|---|
| **STN** | Mallet et al. 2008 [46] | 8 | 32.14 | NA | AC | Tip of the electrode | ±11.30 -9.90 -7.81 |
| **amGPi** | Nair et al. 2014 [12] | 4* | NA | ±14.47 9.85 -3.28 | MCP | Tip of the electrode | ±15.66 -1.41 -8.22 |
| **VC/VS** | Tsai et al. 2010 [47] | 1 | NA | ±7.5 16.3 -3.05 | MCP | Tip of the electrode | ±7.92 5.51 -9.01 |
| **slbMFB** | Coenen et al. 2017 [13] | 2 | 41.7 at 12 months | ±7.6 -1.72 -3.0 | MCP | Active contacts | ±8.35 -13.64 -7.00 |
| **NAc** | Sturm et al. 2003 [5] | 4 | NA | ±6.5 2.5 -4.5 | AC | Tip of the electrode | ±6.98 3.69 −10.55 |
| **ALIC** | Nuttin et al. | 6 | 38.69 | ±13 3.5 0 | AC | Tip of the | ±13.84 5.17 -5.04 |

| DBS Target | Reference | Number of patients | % YBOCS change | AC/PC coordinates | Relative to | Target type | MNI coordinates (Figure 5) |
|---|---|---|---|---|---|---|---|
| | 2003 [48] | | | | | electrode | |
| **MD** | Maarouf et al. 2016 [14] | 4 | 0 | ±4.7 -18.52 4.87 | AC | Active contacts | ±5.10 -18.17 2.59 |
| **VA** | | | | ±6.84 -13.76 7.78 | | | ±7.52 -12.68 5.60 |
| **iml** | | | | ±5.78 -14.9 7.08 | | | ±6.36 -13.99 4.85 |
| **ITP** | Lee et al. 2019 [10] | 5 | 52 | ±6.5 -3 -0.5 | AC | Tip of the electrode | ±6.92 -1.84 -5.13 |
| **BNST** | Nuttin et al. 2013 [49] | 4 | NA | ±6 0 0 | AC | Tip of the electrode | ±6.33 1.39 -4.87 |

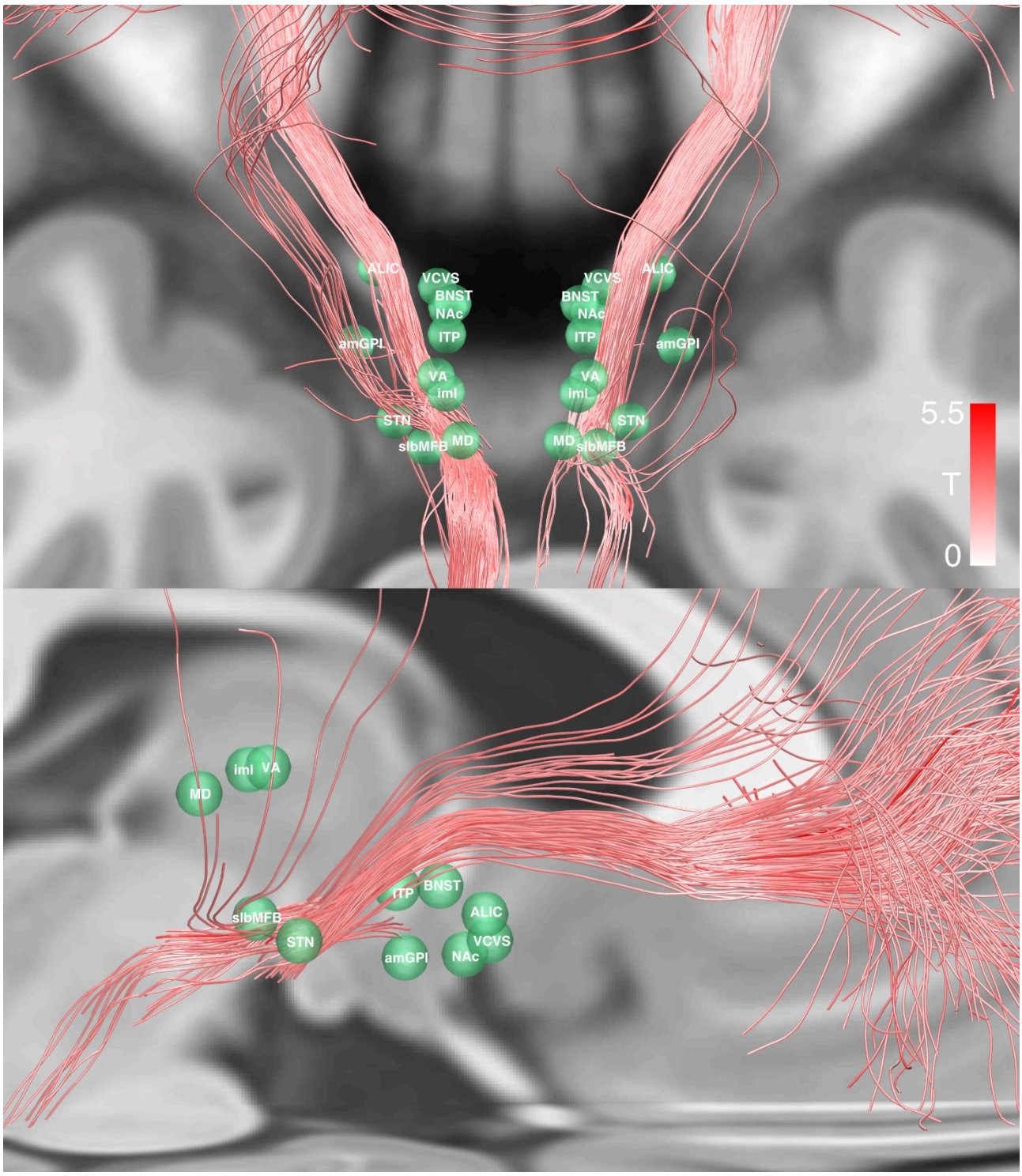


**Figure 5.** Overview of the positively predictive fiber tracts identified in the present study in synopsis with DBS targets for treatment of OCD based on literature results that were mapped to MNI space. Note that most targets were reported for the tip of the electrode, thus, active stimulation may have occurred dorsal to the targets (Table 2).

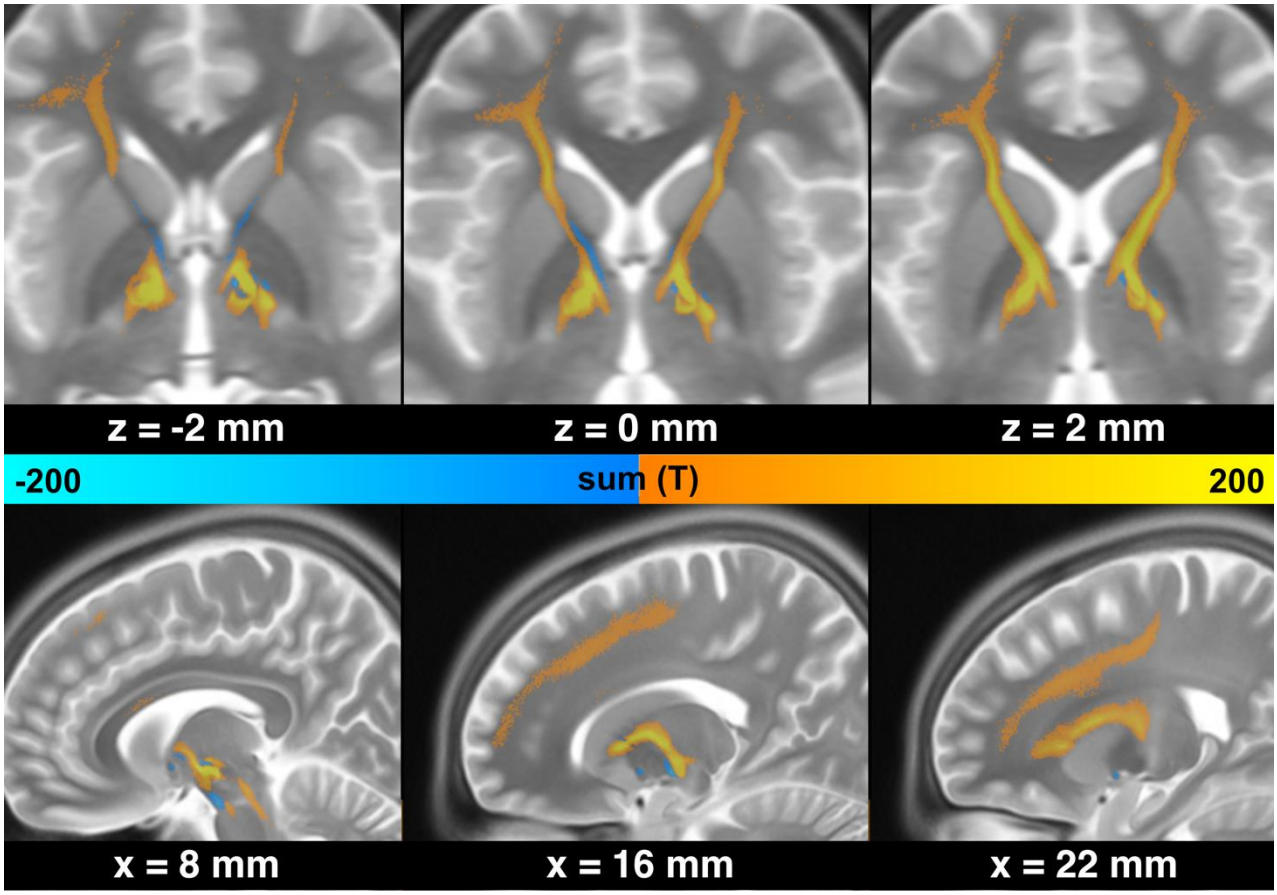


**Figure 6.** Anatomical course of peaks in discriminative fibers shown in MNI space. The tract is connected to the subthalamic nucleus, traverses through the anterior limb of the internal capsule and has connections to medial and lateral prefrontal prefrontal cortex, frontal pole and orbitofrontal cortex.

## Discussion

In the present work, we analyzed data from three cohorts of OCD patients with different DBS targets using a connectomic approach. Strikingly, in both an ALIC-DBS and STN-DBS cohort, the same fiber bundle, which connected the group of VTAs with the dorsal anterior cingulate cortex, ventrolateral and medial prefrontal cortex, was predictive of good clinical improvement. It was possible to cross-predict clinical improvement based on the degree of how strongly the tract was activated in patients across DBS cohorts, targets and centers. Using the estimated tract target, clinical outcome in an independent test sample from a third center, in which patients received electrodes targeting both STN and ALIC, could be predicted.

In recent work by Baldermann et al. 2019 [23], a fiber bundle was identified that was associated with good clinical improvement in OCD when modulated by high-frequency DBS. This bundle connected the medial and lateral prefrontal cortex, dorsal anterior cingulate cortex, subthalamic nucleus and MD nuclei of the thalamus in ALIC-DBS patients. Baldermann and colleagues concluded that DBS would modulate the prefronto-subcortical communication within this fronto-thalamic pathway, which is in line with the assumption that a dysregulation in the fronto-striato-thalamic circuit underlies OCD [50–52].

After seeking advice from colleagues in the anatomy field, we deliberately chose to use descriptive nomenclature for the isolated tract. Despite the high methodological limitations of diffusion MRI based tractography [35,53], it is still possible to say that the isolated tract traverses within the (anterior limb of the) internal capsule (see below). Furthermore, the subthalamic nucleus receives afferents from a large portion of the prefrontal cortex by hyperdirect pathways that are known to traverse within the internal capsule [38,54]. In rodents, lesion to this “limbic hyperdirect pathway” led to diminished discriminative accuracy and increased perseveration [55]. One classical cortical region which was described as an origin of this limbic hyperdirect pathway is the dACC [36,38,56] which crucially plays a prominent role in the classical cortico-striato-thalamo-cortical (CSTC) model of OCD [56] and leads to improvement of OCD symptoms when lesioned in humans [57]. In fact, McGovern & Sheth attributed a central role to the dACC in a novel theory of cognitive control dysfunction [56]. The normative connectome analysis identified the dACC as a cortical connection site to the identified tract. Moreover, when repeating the analysis using an atlas of predefined anatomical tracts [36], the hyperdirect pathway connecting dACC to the STN was isolated from five bundles that traversed the ALIC that were present in the atlas (Figures S1-2). Thus, the cortical input from dACC to STN is a likely anatomical substrate to form part of the identified

bundle. In this context, it is crucial to note that the used atlas by nature could likely not cover all white-matter bundles that are present in the ALIC / STN region and shows “gaps” in between the bundles that traverse within the ALIC. Thus, while the normative connectome definitely includes a large number of false-positive fibers, the atlas could instead be prone to false-negative connections, i.e. some tracts are simply not represented in the atlas. For instance, it is likely that the STN does receive direct input from other areas of the prefrontal cortex such as the ventrolateral prefrontal cortex (which the normative connectome method identified) [58]. In summary, while dACC and vlPFC are likely candidates, our method is unable to determine the exact cortical region(s) of origin of the identified tract with absolute certainty However, it may indeed allow for an accurate three-dimensional reconstruction of the tract itself.

A highly similar pathway that already served as a tract-target in a small case-series of OCD patients [13] also traversed within the ALIC but has instead been referred to as the superolateral branch of the medial forebrain bundle [45]. The anatomical definition of the medial forebrain bundle instead suggests a more ventral route connecting the ventral tegmental area to the olfactory cortex while bypassing the red nucleus medially [39]. In other words, the classical definition of the medial forebrain bundle does not traverse within the ALIC. This mismatch between the surgical target and anatomical literature has recently been described by the original authors and they have now additionally referred to the tract as vtaPP (ventral tegmental area projection pathway) [59]. Given the findings of connectivity between frontal areas and STN described above, especially the ones that are based on the basal ganglia pathway atlas [36], our interpretation differs since we attribute the tract to afferents of the STN as opposed to efferents of the ventral tegmental area. Combining dMRI and tracing methods in nonhuman primates as well as human subjects made it possible to precisely segregate prefrontal fibers passing through the internal capsule [60]. These methods allowed to functionally segment the ALIC and fibers originating from ventrolateral prefrontal cortex (areas 45 and 47) were shown to terminate in the medial part of the STN and the MD nucleus of the thalamus – precisely corresponding to the tract described by Baldermann and colleagues [23] and in the present study.

The linkage between OCD and an imbalance between areas in the frontal cortex and the basal ganglia was further supported by a recent study, showing enhanced cognitive control and theta increases in the medial and lateral PFC after VC/VS DBS in patients with MDD and OCD [61]. Furthermore, the fact that lesions to the dACC in cingulotomy result in OCD symptom improvements [57] further supports a strong role of this region, which is connected

to the STN [36,38,56]. Besides, these changes in frontal oscillations were able to explain clinical outcome. However, as many targets have been used clinically in OCD [15], it is still unclear which target is best and whether the underlying stimulated networks are the same.

## Toward symptom-specific circuitopathies

Based on our results, it seems that two testable hypotheses with implications beyond the STN and ALIC and above and beyond OCD may be proposed. First, based on the joint results of both studies, it seems that (two) different surgical targets may reduce *the same* symptoms equally well – potentially by modulating the same tract or network. Second, it seems that different surgical targets may modulate not only one (shared) network but other networks that are not shared (widely different connectivity profiles of the two targets shown by both studies and differential effects on depressive and cognitive functions described in the Tyagi et al. study). From these two observations, one may derive the concept of symptom-specific networks that – when modulated – do not ameliorate a specific disease but rather specific symptoms that are present in the disease. In OCD, accordingly, different symptom types (for example contamination vs. checking) were found to activate different prefrontal sites (ventromedial vs. dorsolateral, respectively) [62].

Similar observations have been made before in other diseases. For instance, Akram and colleagues demonstrated that connectivity to specific cortical regions is associated with improvement in different clinical features of Parkinson's Disease (e.g. connectivity to M1 preferentially reduced tremor while to the SMA reduced rigidity and bradykinesia) [24]. Another example is the involvement of a cerebello-thalamic pathway for tremor symptom alleviation in both PD and Essential Tremor [63,64].

Our study does not have the aim to analyze which surgical target is potentially better for treatment of OCD – the available clinical data and retrospective design are not well suited to answer this question. However, our study was able to predict symptom-specific clinical improvement *across DBS targets* based on connectivity data. Once more, the tract that our data seems to shape out is predictive for Y-BOCS improvement – but completely different tracts could have emerged when repeating the analyses for depressive or cognitive flexibility symptoms (as analyzed by Tyagi et al.). Unfortunately, these data are not available for the two main cohorts analyzed here. It is likely, that there the two targets do not share tracts that are predictive for improvement in these additional symptoms (e.g. depressive symptoms and cognitive flexibility).

Similar shared symptom networks could be present in different diseases in which various

experimental surgical targets are being investigated. Major Depression and Tourette's Syndrome are obvious candidates and extensive work in this direction is currently ongoing [65–69]. Similar concepts could even be applied to more established targets such as STN vs. GPi DBS [70–72] or symptom-specific alleviations across diseases (e.g. tremor in Parkinson's Disease, Essential Tremor and Dystonic Tremor).

Potentially, DBS surgery in the (distant) future could involve detailed preoperative phenotyping to establish a broad patient-specific symptom score. Based on databases of clinical improvements along the affected symptom axes, *a mix of networks* that could be modulated to alleviate each patient's symptoms could be identified. We must emphasize that this study presents group data and utilizes connectivity from individuals without OCD. As mentioned by others in this very context, we could not agree more that surgical decision making for DBS should not be based on aggregated normative data alone [45]. Further studies are required to determine whether individual patient connectivity or generic connectome data can assist with optimization of surgical targeting by determining the crossing sites of symptom networks for each specific patient.

## Limitations

Several limitations apply for the current work. First and foremost, the retrospective character of the study is not ideal to compare and study effects of clinical outcome which is why we kept clinical information to a minimum and instead referred to clinical studies. Second, we used normative connectome data instead of patient-specific diffusion-weighted MRI data (which is unavailable for most of the patients included). This poses dramatic limitations given that such data cannot be representative of patient-specific anatomical variations. Still, we argue that some aspects about general pathophysiological mechanisms can still be investigated using normative data. Use of normative connectomes has been introduced in other clinical domains where patient-specific MRI data is unavailable, such as stroke [73–75] or transcranial magnetic stimulation [76]. In DBS, the technique has also been applied before and – as in the present study – has led to models that could be used to predict out-of-sample data [18,23,77]. In addition to the practical advantage of being applicable in cases where patient-specific data is lacking, normative data also has the theoretical advantage of much better data quality. In the present case, a connectome dataset was derived from a high N of 985 subjects scanned under research conditions by one of the best methodological groups in the world [78]. Data of such quality can usually not be acquired in individual patients and test-retest scan reliability in DBS settings has shown to be poor even when applying state-of-the-art MRI protocols [79]. However, patient-specific connectivity data is informed by the

individual wiring diagram of each patient's brain – which can never be reconstructed when applying normative connectomes. Potentially, the use of combined information from normative and patient-specific connectomes may embody a promising strategy that could be explored, in the future.

Inaccuracies in lead localization may result from the approach of warping electrodes into common space as done here. To minimize this issue, we used a modern neuroimaging pipeline that has been scientifically validated in numerous studies and involves advanced concepts such as brain shift correction, multispectral normalization, subcortical refinement steps [80] and phantom-validated electrode localizations [81]. The normalization strategy that was applied was found to automatically segment the STN as precisely as manual expert segmentations [82] and each step of the pipeline was carefully assessed and corrected if needed by a team with long-standing expertise in this area [83,84].

Importantly, given the correlative nature of the study, our findings may not differentiate between local and global effects. For instance, the tracts may have spuriously originated in the ALIC group because a more dorsal stimulation resulted with better clinical outcome. The congruency between results of the STN- and ALIC-cohorts resulting in the same fiber bundle may still suggest that the identified tract could play a causal role. However, such a claim would need to be confirmed e.g. using optogenetics in animal studies.

It has been shown that dMRI-based tractography reconstructs a very high proportion of false-positive fibers in recent open challenges [35,53]. We aimed at reducing the risk of false positive tractography results in four ways. First, we used the tracking method that achieved the highest (92%) valid connection score among 96 methods submitted from 20 different research groups in a recent open competition [35]. Second, we used highest quality multi-shell diffusion data [78] acquired on a high N (985 subjects) at a state-of-the-art imaging center (HCP data acquired at Washington University in St. Louis, see Acknowledgements). Third, we compared the tract results with anatomy text-books and discussed its validity with four anatomists (see Acknowledgements). Fourth, we replicated findings based on an atlas that is based on predefined anatomical tracts (see supplementary material). The tract described in the present study matches results from this atlas (Figure S1-2) and dissection studies (Figure S4). However, the potential that the tract represents a false positive result may not be completely ruled out given the fundamental limitations of dMRI-based tractography [35,53].

## Conclusions

Three main conclusions may be drawn from the present study. First, we show that the overall

connectivity profiles of STN- and ALIC-DBS electrodes project to largely different areas in the brain. Second, results of each cohort separately singled out the same fiber tract that was associated with long-term improvement of OCD symptoms when modulated either at the level of the STN or the ALIC. Third, we demonstrated that it is possible to cross-predict clinical improvement of OCD patients across DBS target sites (ALIC / STN) and centers (Cologne / Grenoble).

# Methods

## Patient Cohorts and Imaging

Forty-two OCD patients from three centers were retrospectively enrolled in this study, among them twenty-two patients from University Hospital of Cologne implanted for ALIC DBS, fourteen patients from Grenoble University Hospital who underwent STN DBS surgery and six patients who received electrodes to both STN and ALIC from the National Hospital for Neurology and Neurosurgery. All patients from Grenoble were bilaterally implanted with DBS electrodes 3389, as were all but three patients from Cologne, who were implanted with type 3387 electrodes (Medtronic, Minneapolis, Minnesota, US). Patients from London received models 3389 to the STN and 3387 to the ALIC. All patients qualified for DBS surgery based on their diagnoses of treatment-resistant severe OCD [16,23,29]. Severity of OCD was assessed both pre- and postoperatively with the Yale-Brown Obsessive-Compulsive Scale (Y-BOCS). Postoperative assessment took place 12 months after surgery. In case of the London cohort, this followed a four-step clinical trial (2x3 months blinded stimulation at one target followed by 6 months of stimulation at both targets, the last three months using clinically optimized parameters. For details see [16]). Patients' demographic details are provided in Table 1. All patients gave written informed consent. The protocols were approved by the Ethics Committee of the University of Cologne and the Ethics Committee of Grenoble University Hospital, respectively.

For all patients in the three cohorts, high-resolution structural T1-weighted images were acquired on a 3.0-Tesla MRI-scanner, before surgery. Postoperative computer tomography (CT) was obtained in twenty-five patients after surgery to verify correct electrode placement, while eleven patients from the Grenoble cohort and the six London patients received postoperative MRI instead.

## DBS Lead Localization and VTA Estimation

DBS electrodes were localized using Lead-DBS software (http://www.lead-dbs.org) as described in [83] and [80]. Briefly, postoperative CT and MRI scans were linearly coregistered to preoperative T1 images using Advanced Normalization Tools (ANTs, http://stnava.github.io/ANTs/) [85]. Subcortical refinement was applied (as a module in Lead-DBS) to correct for brain shift that may have occurred during surgery. Images were then normalized into ICBM 2009b Nonlinear Asymmetric ("MNI") template [34] space using the SyN approach implemented in ANTs [86], with an additional subcortical refinement stage to attain

a most precise subcortical alignment between patient and template space ("Effective Low Variance" preset as implemented in Lead-DBS). Of note, this specific method was the top performer for subcortical image registrations in a recent comparative study that involved >10,000 nonlinear warps and a variety of normalization techniques [82]. Both coregistrations and normalizations were visually reviewed and refined if needed. DBS electrodes were then localized using Lead-DBS and warped into MNI space.

In the Grenoble and Cologne groups, Volumes of Tissue Activated (VTA) were estimated using a finite element method (FEM) as described in [80]. Briefly, a volume conductor model was constructed based on a four-compartment mesh that included gray matter, white matter, electrode contacts and insulated parts. Gray matter was defined by the CIT-168 [32] and DISTAL [33] atlases for the ALIC- and STN-cohorts, respectively. These atlases were specifically adapted or created for use within the Lead-DBS pipeline. The electric field (E-field) distribution was then simulated using an adaptation of the FieldTrip-SimBio pipeline [87] that was integrated into Lead-DBS (https://www.mrt.uni-jena.de/simbio/; http://fieldtriptoolbox.org/) and thresholded at a level of 0.2 V/m [80].

For the London test cohort, we chose to use the original VTAs of the published study by Tyagi et al. [16]. These had been processed using Medtronic SureTune™ software and had been transferred into MNI space within the original study. The reason we chose to use the original VTAs were twofold. First, it would demonstrate generalizability of our findings (i.e. that our results could still be useful in case electrodes were localized using different software). Second, we aimed at yielding maximal transferability to the study by Tyagi et al. which reported on the rich London dataset in more depth.

## Connectivity Analysis

Structural connectivity between VTAs and all other brain areas was calculated based on a normative connectome as similarly done in previous work [18,23,33,37,77,80]. Specifically, a whole-brain connectome based on state-of-the-art multi-shell diffusion-weighted imaging data from 985 subjects of the Human Connectome Project (HCP) 1200 subjects data release [78] was calculated in each patient using Lead-Connectome. Whole-brain fiber tracts were then normalized into standard space using a multispectral warp based on T1-weighted, T2-weighted, and diffusion-weighted acquisitions using ANTs (using the same "Effective Low Variance" preset implemented in Lead-DBS). In each subject, a total of 6,000 fibers were sampled and aggregated to a joint dataset in standard space. From this, a set of 6,000,000

fibers across 985 HCP subjects were accumulated for analysis in this study. For each of these tracts, a “Fiber T-score” was assigned by associating the fiber tract’s connectivity to VTAs across patients with clinical outcome (Figure 7). Specifically, (mass-univariate) two-sample t-tests between clinical outcomes in connected and unconnected VTAs were performed for all 6,000,000 tracts. Needless to say, these T-scores were not meant to result in significant results but instead formed a model that could be used for out-of-sample predictions in the other DBS cohort. The Fiber T-scores were then defined as the T-values from these tests and could be positive or negative (since two-sided t-tests were performed). A high absolute T-score meant that the fiber was strongly discriminative or predictive for clinical outcome. For instance, a tract that was connected exclusively to VTAs in good responders (and not to VTAs of poor responders) would receive a high positive T-score (termed “Fiber T-score” below). In return, a patient would most likely show more pronounced clinical benefit, if her/his VTA was strongly connected to fibers with high positive T-scores.

To account for the fact that larger VTAs would potentially automatically receive higher T-scores, reported Fiber T-scores were divided by the stimulation amplitude throughout the manuscript. Random permutation ($\times$ 5000) was conducted to obtain *p*-values, except for two-sample T-Tests.

In figures of this manuscript, fibers were color-coded by their associated T-scores. A schematic overview of the above described method is shown in Figure 7. Only highly predictive fibers were kept (top 20% based on Fiber T-scores), which formed the “discriminative fiber set”. Based on the discriminative fiber set, the association between the fiber connectivity and the clinical outcome was analyzed. For instance, in the main analysis, a discriminative fiber set was defined exclusively on the ALIC cohort but was then used to predict outcome in patients from the STN cohort (and vice-versa). To do so, the T-scores of connected fibers from the discriminative fiber set were summed up for each patient and this value was correlated with the clinical improvement, as measured by the %-improvement of Y-BOCS scores between preoperative and 12 months postoperative assessments. Scatterplots in the present manuscript are visualized with 95% confidence bounds (gray or light-red areas).

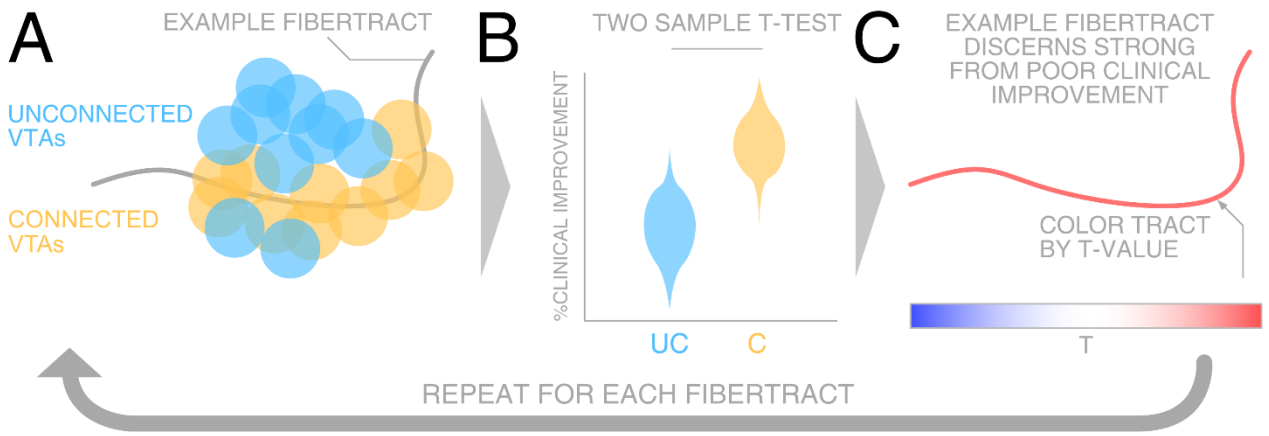


**Figure 7.** Summary of methods to define a Fiber T-score for each tract. A) For each fiber, VTAs were grouped into either connected (C; yellow) or unconnected (UC; blue) sets across patients. B) Two-sample t-tests between clinical improvements in connected and unconnected VTAs were calculated in a mass-univariate fashion for each fiber tract separately. C) The resulting Fiber T-score of this analysis leads to the “weight” that each fiber is given, as well as the color in visualizations throughout the manuscript. Here, red means that the fiber tract is favorably connected to good responders while blue indicates the opposite (and the saturation of tracts denotes how discriminative they are).

## Data and code availability

The DBS MRI datasets generated during and analyzed during the current study are not publicly available due to data privacy regulations of patient data but are available from the corresponding author on reasonable request. All code used to analyze the dataset is available within Lead-DBS /-Connectome software (https://github.com/leaddbs/leaddbs).

## References

1. Ruscio, A. M., Stein, D. J., Chiu, W. T. & Kessler, R. C. The epidemiology of obsessive-compulsive disorder in the National Comorbidity Survey Replication. *Mol. Psychiatry* **15**, 53–63 (2010).
2. Mallet, L. *et al.* Compulsions, Parkinson's disease, and stimulation. *The Lancet* **360**, 1302–1304 (2002).
3. Chabardès, S. *et al.* Deep Brain Stimulation for Obsessive-Compulsive Disorder: Subthalamic Nucleus Target. *World Neurosurg.* **80**, S31.e1-S31.e8 (2013).
4. Anderson, D. & Ahmed, A. Treatment of patients with intractable obsessive—compulsive disorder with anterior capsular stimulation: Case report. *J. Neurosurg.* **98**, 1104–1108 (2003).
5. Sturm, V. *et al.* The nucleus accumbens: a target for deep brain stimulation in obsessive–compulsive- and anxiety-disorders. *J. Chem. Neuroanat.* **26**, 293–299 (2003).
6. Aouizerate, B. *et al.* Deep brain stimulation of the ventral caudate nucleus in the treatment of obsessive—compulsive disorder and major depression: Case report. *J. Neurosurg.* **101**, 682–686 (2004).
7. Franzini, A. *et al.* Deep-brain stimulation of the nucleus accumbens in obsessive compulsive disorder: clinical, surgical and electrophysiological considerations in two consecutive patients. *Neurol. Sci.* **31**, 353–359 (2010).
8. Greenberg, B. D. *et al.* Three-Year Outcomes in Deep Brain Stimulation for Highly Resistant Obsessive–Compulsive Disorder. *Neuropsychopharmacology* **31**, 2384–2393 (2006).
9. Jiménez-Ponce, F. *et al.* Preliminary Study in Patients With Obsessive-Compulsive Disorder Treated With Electrical Stimulation in the Inferior Thalamic Peduncle. *Oper. Neurosurg.* **65**, ons203–ons209 (2009).
10. Lee, D. J. *et al.* Inferior thalamic peduncle deep brain stimulation for treatment-refractory obsessive-compulsive disorder: A phase 1 pilot trial. *Brain Stimulat.* **12**, 344–352 (2019).
11. Luyten, L., Hendrickx, S., Raymaekers, S., Gabriëls, L. & Nuttin, B. Electrical stimulation in the bed nucleus of the stria terminalis alleviates severe obsessive-compulsive disorder. *Mol. Psychiatry* **21**, 1272–1280 (2016).
12. Nair, G., Evans, A., Bear, R. E., Velakoulis, D. & Bittar, R. G. The anteromedial GPi as a new target for deep brain stimulation in obsessive compulsive disorder. *J. Clin. Neurosci.* **21**, 815–821 (2014).
13. Coenen, V. A. *et al.* The medial forebrain bundle as a target for deep brain stimulation for obsessive-compulsive disorder. *CNS Spectr.* **22**, 282–289 (2017).
14. Maarouf, M. *et al.* Deep Brain Stimulation of Medial Dorsal and Ventral Anterior Nucleus of the Thalamus in OCD: A Retrospective Case Series. *PLOS ONE* **11**, e0160750 (2016).
15. Borders, C., Hsu, F., Sweidan, A. J., Matei, E. S. & Bota, R. G. Deep brain stimulation for obsessive compulsive disorder: A review of results by anatomical target. *Ment. Illn.* **10**, (2018).
16. Tyagi, H. *et al.* A Randomized Trial Directly Comparing Ventral Capsule and Anteromedial Subthalamic Nucleus Stimulation in Obsessive-Compulsive Disorder: Clinical and Imaging Evidence for Dissociable Effects. *Biol. Psychiatry* (2019) doi:10.1016/j.biopsych.2019.01.017.
17. Lozano, A. M. & Lipsman, N. Probing and Regulating Dysfunctional Circuits Using Deep Brain Stimulation. *Neuron* **77**, 406–424 (2013).
18. Horn, A. *et al.* Connectivity Predicts deep brain stimulation outcome in Parkinson disease. *Ann. Neurol.* **82**, 67–78 (2017).
19. Horn, A. The impact of modern-day neuroimaging on the field of deep brain stimulation. *Curr. Opin. Neurol.* **Publish Ahead of Print**, (2019).
20. Schaerer, J., Roche, F. & Belaroussi, B. A generic interpolator for multi-label images. *Insight J.* 950 (2014).
21. Liebrand, L. C. *et al.* Individual white matter bundle trajectories are associated with deep brain stimulation response in obsessive-compulsive disorder. *Brain Stimulat.* **12**, 353–360 (2019).
22. Heilbronner, S. R., Safadi, Z. & Haber, S. N. Neurocircuits commonly involved in psychiatric

disorders and their stimulation and lesion therapies. in *Neuromodulation in Psychiatry* 27–48 (John Wiley & Sons, Ltd, 2016). doi:10.1002/9781118801086.ch3.
23. Baldermann, J. C. *et al.* Connectivity profile predictive of effective deep brain stimulation in obsessive compulsive disorder. *Biol. Psychiatry* (2019) doi:10.1016/j.biopsych.2018.12.019.
24. Akram, H. *et al.* Subthalamic deep brain stimulation sweet spots and hyperdirect cortical connectivity in Parkinson's disease. *NeuroImage* **158**, 332–345 (2017).
25. Middlebrooks, E. H. *et al.* Segmentation of the Globus Pallidus Internus Using Probabilistic Diffusion Tractography for Deep Brain Stimulation Targeting in Parkinson Disease. *Am. J. Neuroradiol.* **39**, 1127–1134 (2018).
26. Vanegas-Arroyave, N. *et al.* Tractography patterns of subthalamic nucleus deep brain stimulation. *Brain* **139**, 1200–1210 (2016).
27. Deuschl, G. *et al.* A Randomized Trial of Deep-Brain Stimulation for Parkinson's Disease. *N. Engl. J. Med.* **355**, 896–908 (2006).
28. Ostrem, J. L. *et al.* Subthalamic nucleus deep brain stimulation in primary cervical dystonia. *Neurology* **76**, 870–878 (2011).
29. Polosan, M. *et al.* Affective modulation of the associative-limbic subthalamic nucleus: deep brain stimulation in obsessive–compulsive disorder. *Transl. Psychiatry* **9**, 73 (2019).
30. Vissani, M., Cordella, R., Micera, S., Romito, L. M. & Mazzoni, A. Spatio-temporal structure of single neuron subthalamic activity in Tourette Syndrome explored during DBS procedures. *bioRxiv* 532200 (2019) doi:10.1101/532200.
31. Alkemade, A., Groot, J. M. & Forstmann, B. U. Do We Need a Human post mortem Whole-Brain Anatomical Ground Truth in in vivo Magnetic Resonance Imaging? *Front. Neuroanat.* **12**, (2018).
32. Pauli, W. M., Nili, A. N. & Tyszka, J. M. A high-resolution probabilistic *in vivo* atlas of human subcortical brain nuclei. *Sci. Data* **5**, 180063 (2018).
33. Ewert, S. *et al.* Toward defining deep brain stimulation targets in MNI space: A subcortical atlas based on multimodal MRI, histology and structural connectivity. *NeuroImage* **170**, 271–282 (2018).
34. Fonov, V., Evans, A., McKinstry, R., Almli, C. & Collins, D. Unbiased nonlinear average age-appropriate brain templates from birth to adulthood. *NeuroImage* **47**, S102 (2009).
35. Maier-Hein, K. H. *et al.* The challenge of mapping the human connectome based on diffusion tractography. *Nat. Commun.* **8**, 1349 (2017).
36. Petersen, M. V. *et al.* Holographic Reconstruction of Axonal Pathways in the Human Brain. *Neuron* **104**, 1056-1064.e3 (2019).
37. Horn, A. *et al.* Probabilistic conversion of neurosurgical DBS electrode coordinates into MNI space. *NeuroImage* **150**, 395–404 (2017).
38. Haynes, W. I. A. & Haber, S. N. The Organization of Prefrontal-Subthalamic Inputs in Primates Provides an Anatomical Substrate for Both Functional Specificity and Integration: Implications for Basal Ganglia Models and Deep Brain Stimulation. *J. Neurosci.* **33**, 4804–4814 (2013).
39. Nieuwenhuys, R., Voogd, J. & van Huijzen, C. *The Human Central Nervous System*. (Springer Berlin Heidelberg, 2008). doi:10.1007/978-3-540-34686-9.
40. McIntyre, C. C. & Hahn, P. J. Network Perspectives on the Mechanisms of Deep Brain Stimulation. *Neurobiol. Dis.* **38**, 329–337 (2010).
41. Nambu, A., Tokuno, H. & Takada, M. Functional significance of the cortico–subthalamo–pallidal 'hyperdirect' pathway. *Neurosci. Res.* **43**, 111–117 (2002).
42. Hartmann, C. J. *et al.* Tractography Activation Patterns in Dorsolateral Prefrontal Cortex Suggest Better Clinical Responses in OCD DBS. *Neuroprosthetics* 519 (2016) doi:10.3389/fnins.2015.00519.
43. Figee, M. *Moving the brain: Neuroimaging motivational changes of deep brain stimulation in obsessive-compulsive disorder*. (2013).
44. Huff, W. *et al.* Unilateral deep brain stimulation of the nucleus accumbens in patients with treatment-resistant obsessive-compulsive disorder: Outcomes after one year. *Clin. Neurol.*

*Neurosurg.* **112**, 137–143 (2010).
45. Coenen, V. A. *et al.* Surgical decision making for deep brain stimulation should not be based on aggregated normative data mining. *Brain Stimul. Basic Transl. Clin. Res. Neuromodulation* **0**, (2019).
46. Mallet, L. *et al.* Subthalamic Nucleus Stimulation in Severe Obsessive–Compulsive Disorder. *N. Engl. J. Med.* **359**, 2121–2134 (2008).
47. Tsai, H.-C., Chen, S.-Y., Tsai, S.-T., Hung, H.-Y. & Chang, C.-H. Hypomania Following Bilateral Ventral Capsule Stimulation in a Patient with Refractory Obsessive-Compulsive Disorder. *Biol. Psychiatry* **68**, e7–e8 (2010).
48. Nuttin, B. J. *et al.* Long-term Electrical Capsular Stimulation in Patients with Obsessive-Compulsive Disorder. *Neurosurgery* **52**, 1263–1274 (2003).
49. Nuttin, B. *et al.* Targeting Bed Nucleus of the Stria Terminalis for Severe Obsessive-Compulsive Disorder: More Unexpected Lead Placement in Obsessive-Compulsive Disorder than in Surgery for Movement Disorders. *World Neurosurg.* **80**, S30.e11-S30.e16 (2013).
50. Bourne, S. K., Eckhardt, C. A., Sheth, S. A. & Eskandar, E. N. Mechanisms of deep brain stimulation for obsessive compulsive disorder: effects upon cells and circuits. *Front. Integr. Neurosci.* **6**, (2012).
51. Figee, M. *et al.* Deep brain stimulation restores frontostriatal network activity in obsessive-compulsive disorder. *Nat. Neurosci.* **16**, 386–387 (2013).
52. Dunlop, K. *et al.* Reductions in Cortico-Striatal Hyperconnectivity Accompany Successful Treatment of Obsessive-Compulsive Disorder with Dorsomedial Prefrontal rTMS. *Neuropsychopharmacology* **41**, 1395–1403 (2016).
53. Schilling, K. G. *et al.* Challenges in diffusion MRI tractography – Lessons learned from international benchmark competitions. *Magn. Reson. Imaging* **57**, 194–209 (2019).
54. Nougaret, S., Meffre, J., Duclos, Y., Breysse, E. & Pelloux, Y. First evidence of a hyperdirect prefrontal pathway in the primate: precise organization for new insights on subthalamic nucleus functions. *Front. Comput. Neurosci.* **7**, (2013).
55. Chudasama, Y., Baunez, C. & Robbins, T. W. Functional Disconnection of the Medial Prefrontal Cortex and Subthalamic Nucleus in Attentional Performance: Evidence for Corticosubthalamic Interaction. *J. Neurosci.* **23**, 5477–5485 (2003).
56. McGovern, R. A. & Sheth, S. A. Role of the dorsal anterior cingulate cortex in obsessive-compulsive disorder: converging evidence from cognitive neuroscience and psychiatric neurosurgery. *J. Neurosurg.* **126**, 132–147 (2017).
57. Dougherty, D. D. *et al.* Prospective Long-Term Follow-Up of 44 Patients Who Received Cingulotomy for Treatment-Refractory Obsessive-Compulsive Disorder. *Am. J. Psychiatry* **159**, 269–275 (2002).
58. Parent, A. & Hazrati, L.-N. Functional anatomy of the basal ganglia. II. The place of subthalamic nucleus and external pallidium in basal ganglia circuitry. *Brain Res. Rev.* **20**, 128–154 (1995).
59. Coenen, V. A. *et al.* Tractographic description of major subcortical projection pathways passing the anterior limb of the internal capsule. Corticopetal organization of networks relevant for psychiatric disorders. *NeuroImage Clin.* **25**, 102165 (2020).
60. Safadi, Z. *et al.* Functional Segmentation of the Anterior Limb of the Internal Capsule: Linking White Matter Abnormalities to Specific Connections. *J. Neurosci.* **38**, 2106–2117 (2018).
61. Widge, A. S. *et al.* Deep brain stimulation of the internal capsule enhances human cognitive control and prefrontal cortex function. *Nat. Commun.* **10**, 1536 (2019).
62. Mataix-Cols, D. *et al.* Distinct Neural Correlates of Washing, Checking, and Hoarding SymptomDimensions in Obsessive-compulsive Disorder. *Arch. Gen. Psychiatry* **61**, 564–576 (2004).
63. Calabrese, E. *et al.* Postmortem diffusion MRI of the human brainstem and thalamus for deep brain stimulator electrode localization. *Hum. Brain Mapp.* **36**, 3167–3178 (2015).
64. Middlebrooks, E. H. *et al.* Structural connectivity–based segmentation of the thalamus and

prediction of tremor improvement following thalamic deep brain stimulation of the ventral intermediate nucleus. *NeuroImage Clin.* **20**, 1266–1273 (2018).
65. Choi, K. S. Characterizing structural neural networks in major depressive disorder using diffusion tensor imaging. (Georgia Institute of Technology, 2013).
66. Choi, K. S., Riva-Posse, P., Gross, R. E. & Mayberg, H. S. Mapping the "Depression Switch" During Intraoperative Testing of Subcallosal Cingulate Deep Brain Stimulation. *JAMA Neurol.* **72**, 1252–1260 (2015).
67. Mayberg, H. S. *et al.* Deep Brain Stimulation for Treatment-Resistant Depression. *Neuron* **45**, 651–660 (2005).
68. Schlaepfer, T. E., Bewernick, B. H., Kayser, S., Mädler, B. & Coenen, V. A. Rapid Effects of Deep Brain Stimulation for Treatment-Resistant Major Depression. *Biol. Psychiatry* **73**, 1204–1212 (2013).
69. Schlaepfer, T. E., Bewernick, B. H., Kayser, S., Hurlemann, R. & Coenen, V. A. Deep Brain Stimulation of the Human Reward System for Major Depression—Rationale, Outcomes and Outlook. *Neuropsychopharmacology* **39**, 1303–1314 (2014).
70. Follett, K. A. *et al.* Pallidal versus Subthalamic Deep-Brain Stimulation for Parkinson's Disease. *http://dx.doi.org/10.1056/NEJMoa0907083* https://www.nejm.org/doi/10.1056/NEJMoa0907083?url_ver=Z39.88-2003&rfr_id=ori%3Arid%3Acrossref.org&rfr_dat=cr_pub%3Dwww.ncbi.nlm.nih.gov (2010) doi:10.1056/NEJMoa0907083.
71. Odekerken, V. J. *et al.* Subthalamic nucleus versus globus pallidus bilateral deep brain stimulation for advanced Parkinson's disease (NSTAPS study): a randomised controlled trial. *Lancet Neurol.* **12**, 37–44 (2013).
72. Odekerken, V. J. J. *et al.* GPi vs STN deep brain stimulation for Parkinson disease: Three-year follow-up. *Neurology* **86**, 755–761 (2016).
73. Darby, R. R., Horn, A., Cushman, F. & Fox, M. D. Lesion network localization of criminal behavior. *Proc. Natl. Acad. Sci. U. S. A.* **115**, 601–606 (2018).
74. Joutsa, J., Horn, A., Hsu, J. & Fox, M. D. Localizing parkinsonism based on focal brain lesions. *Brain* **141**, 2445–2456 (2018).
75. Joutsa, J. *et al.* Identifying therapeutic targets from spontaneous beneficial brain lesions. *Ann. Neurol.* **84**, 153–157 (2018).
76. Weigand, A. *et al.* Prospective Validation That Subgenual Connectivity Predicts Antidepressant Efficacy of Transcranial Magnetic Stimulation Sites. *Biol. Psychiatry* **84**, 28–37 (2018).
77. Neumann, W.-J. *et al.* Functional segregation of basal ganglia pathways in Parkinson's disease. *Brain* **141**, 2655–2669 (2018).
78. Van Essen, D. C. *et al.* The WU-Minn Human Connectome Project: An overview. *NeuroImage* **80**, 62–79 (2013).
79. Petersen, M. V. *et al.* Probabilistic versus deterministic tractography for delineation of the cortico-subthalamic hyperdirect pathway in patients with Parkinson disease selected for deep brain stimulation. *J. Neurosurg.* **126**, 1657–1668 (2017).
80. Horn, A. *et al.* Lead-DBS v2: Towards a comprehensive pipeline for deep brain stimulation imaging. *NeuroImage* **184**, 293–316 (2019).
81. Husch, A., V. Petersen, M., Gemmar, P., Goncalves, J. & Hertel, F. PaCER - A fully automated method for electrode trajectory and contact reconstruction in deep brain stimulation. *NeuroImage Clin.* **17**, 80–89 (2017).
82. Ewert, S. *et al.* Optimization and comparative evaluation of nonlinear deformation algorithms for atlas-based segmentation of DBS target nuclei. *NeuroImage* **184**, 586–598 (2019).
83. Horn, A. & Kühn, A. A. Lead-DBS: A toolbox for deep brain stimulation electrode localizations and visualizations. *NeuroImage* **107**, 127–135 (2015).
84. Schönecker, T., Kupsch, A., Kühn, A. A., Schneider, G.-H. & Hoffmann, K.-T. Automated Optimization of Subcortical Cerebral MR Imaging−Atlas Coregistration for Improved Postoperative Electrode Localization in Deep Brain Stimulation. *Am. J. Neuroradiol.* **30**, 1914–1921 (2009).

85. Avants, B. B., Tustison, N. & Song, G. Advanced normalization tools (ANTS). *Insight J* **2**, 1–35 (2009).
86. Avants, B. B., Epstein, C. L., Grossman, M. & Gee, J. C. Symmetric Diffeomorphic Image Registration with Cross-Correlation: Evaluating Automated Labeling of Elderly and Neurodegenerative Brain. *Med. Image Anal.* **12**, 26–41 (2008).
87. Vorwerk, J., Oostenveld, R., Piastra, M. C., Magyari, L. & Wolters, C. H. The FieldTrip-SimBio pipeline for EEG forward solutions. *Biomed. Eng. OnLine* **17**, 37 (2018).
88. Morel, A. *Stereotactic Atlas of the Human Thalamus and Basal Ganglia*. (CRC Press, 2007). doi:10.3109/9781420016796.

## Acknowledgements

This work was supported by the German Research Foundation (Deutsche Forschungsgemeinschaft, Emmy Noether Stipend 410169619 to AH, KFO 247 to AAK and KFO 219 to JK). We would like to thank Kristy Kultas-Ilinsky and Igor Ilinsky, Rudolf Nieuwenhuys and Suzanne Haber for counceling regarding the anatomical validity of tractography results presented in this study.

Data were provided [in part] by the Human Connectome Project, WU-Minn Consortium (Principal Investigators: David Van Essen and Kamil Ugurbil; 1U54MH091657) funded by the 16 NIH Institutes and Centers that support the NIH Blueprint for Neuroscience Research; and by the McDonnell Center for Systems Neuroscience at Washington University.

## Author contributions

A. H., N.L. and A.A.K. conceptualized the study. A.H. and N.L. developed the software pipeline used, analyzed data and wrote the manuscript. J.C.B. conceptualized the study, acquired patient data and revised the manuscript. S.T. co-wrote the manuscript. A.K., acquired data and revised the manuscript. H.A. acquired and processed patient data and revised the manuscript. S.C. V.V.V. M.P. J.K., L.Z. and E.J. acquired patient data and revised the manuscript. G.J.B.E., A.B., and A.M.L. processed and analyzed human connectome data and revised the manuscript.

## Competing interests

A.H. reports one-time lecture fee for Medtronic. A.A.K. reports personal fees and non-financial support from Medtronic, personal fees from Boston Scientific, grants and personal fees from Abbott outside the submitted work. A.M.L. is consultant for Medtronic, Abbott and Boston Scientific. M.P. has received honoraria for lecturing from the Movement Disorder Society, Medtronic, research support from Boston Scientific. S.C. is consultant for Medtronic, Boston Scientific and Zimmer Biomet. JK has received financial support for investigator-initiated trials from Medtronic. A.B., A.K., E.J., G.J.B.E., H.A., J.C.B., L.Z., N.L., S.T. and V.V.V. have nothing to disclose.

## Materials & Correspondences

Correspondence and material requests should be addressed to Ningfei Li (ningfei.li@charite.de)

## Supplementary Material

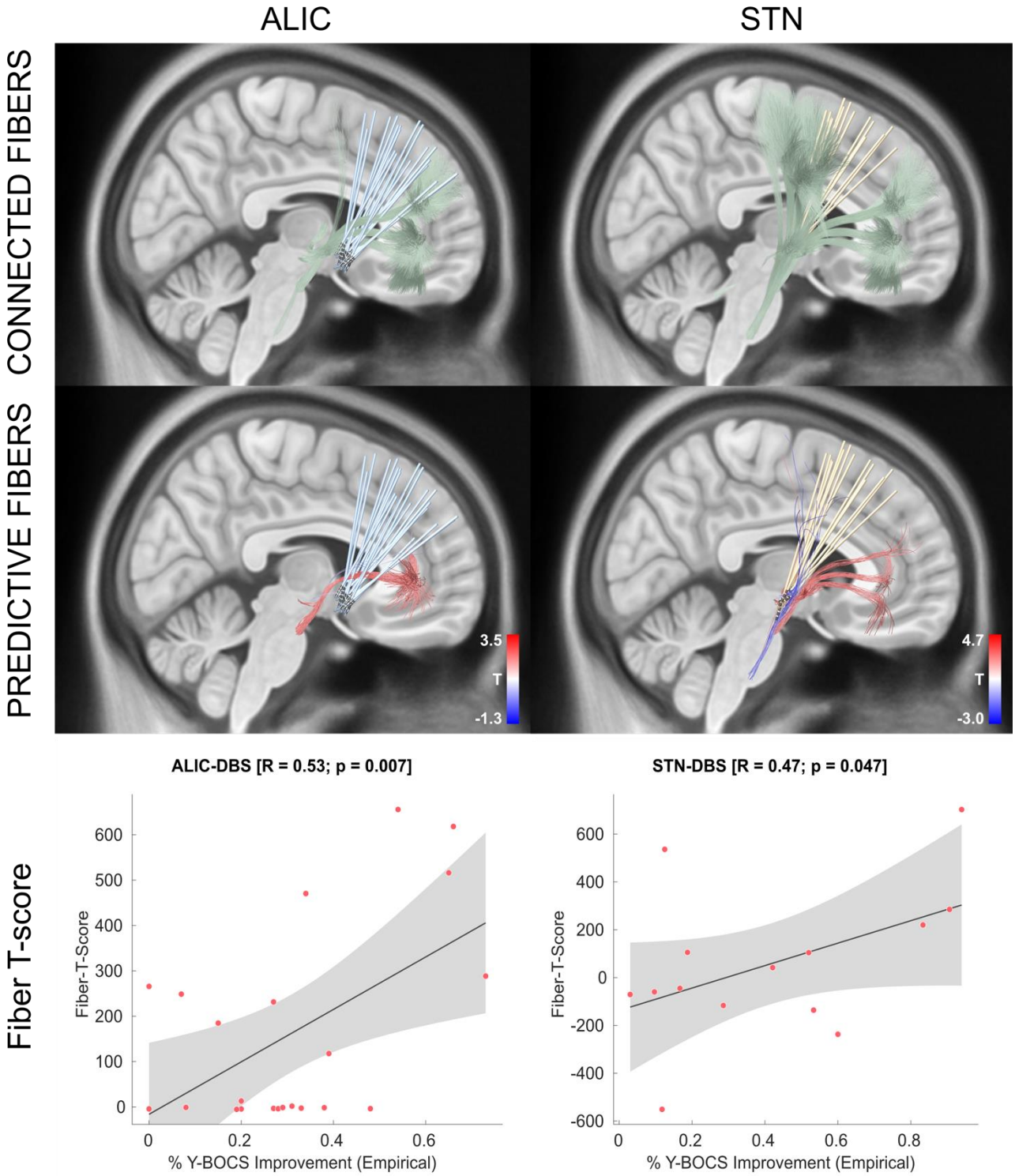


**Figure S1.** Replication of Figure 2 using the basal ganglia pathway atlas [36] instead of a normative connectome. This atlas is not based on diffusion-weighted imaging but on established anatomical expert knowledge and is thus free from false-positive connections. While the STN target isolates three distinct bundles that traverse within the ALIC, the most predictive bundle isolated by the ALIC electrodes is the hyperdirect pathway connecting dACC and STN. In this context, it is crucial to note that connections from other regions of the prefrontal cortex (such as the ventrolateral or medial prefrontal cortex) to the STN were not represented in the atlas (and could thus represent false-negative findings, as shown by the

white-matter gaps between atlas components).

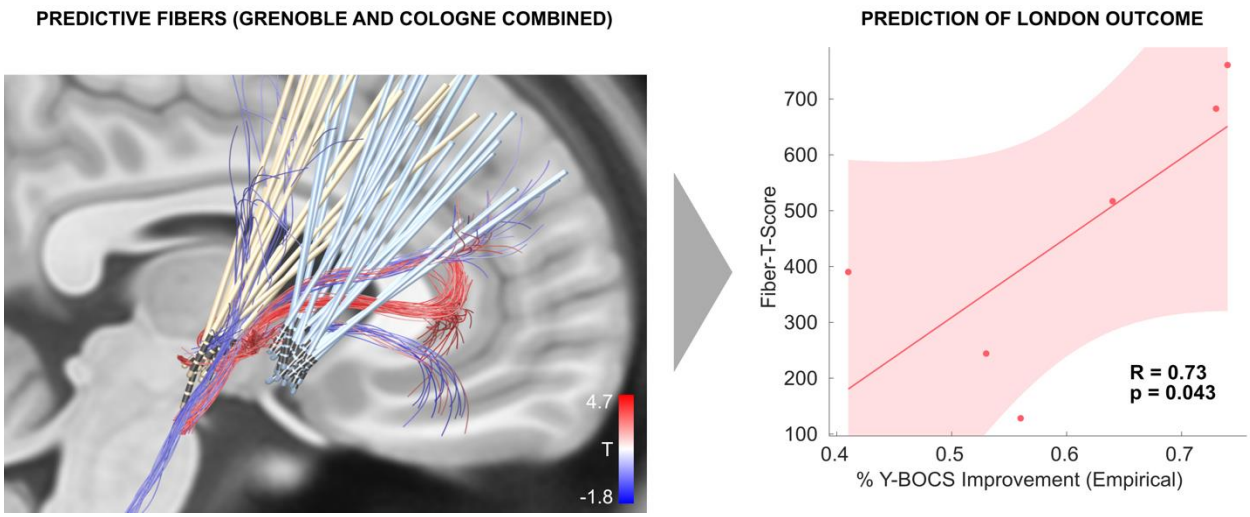


**Figure S2.** Replication of Figure 4 using the basal ganglia pathway atlas [36] instead of a normative connectome. This atlas is not based on diffusion-weighted imaging but on established anatomical expert knowledge and is thus free from false-positive connections. The most predictive bundle present in the atlas was the hyperdirect pathway connecting dACC and STN. In this context, it is crucial to note that connections from other regions of the prefrontal cortex (such as the ventrolateral or medial prefrontal cortex) to the STN were not represented in the atlas (and could thus represent false-negative findings, as shown by the white-matter gaps between atlas components).

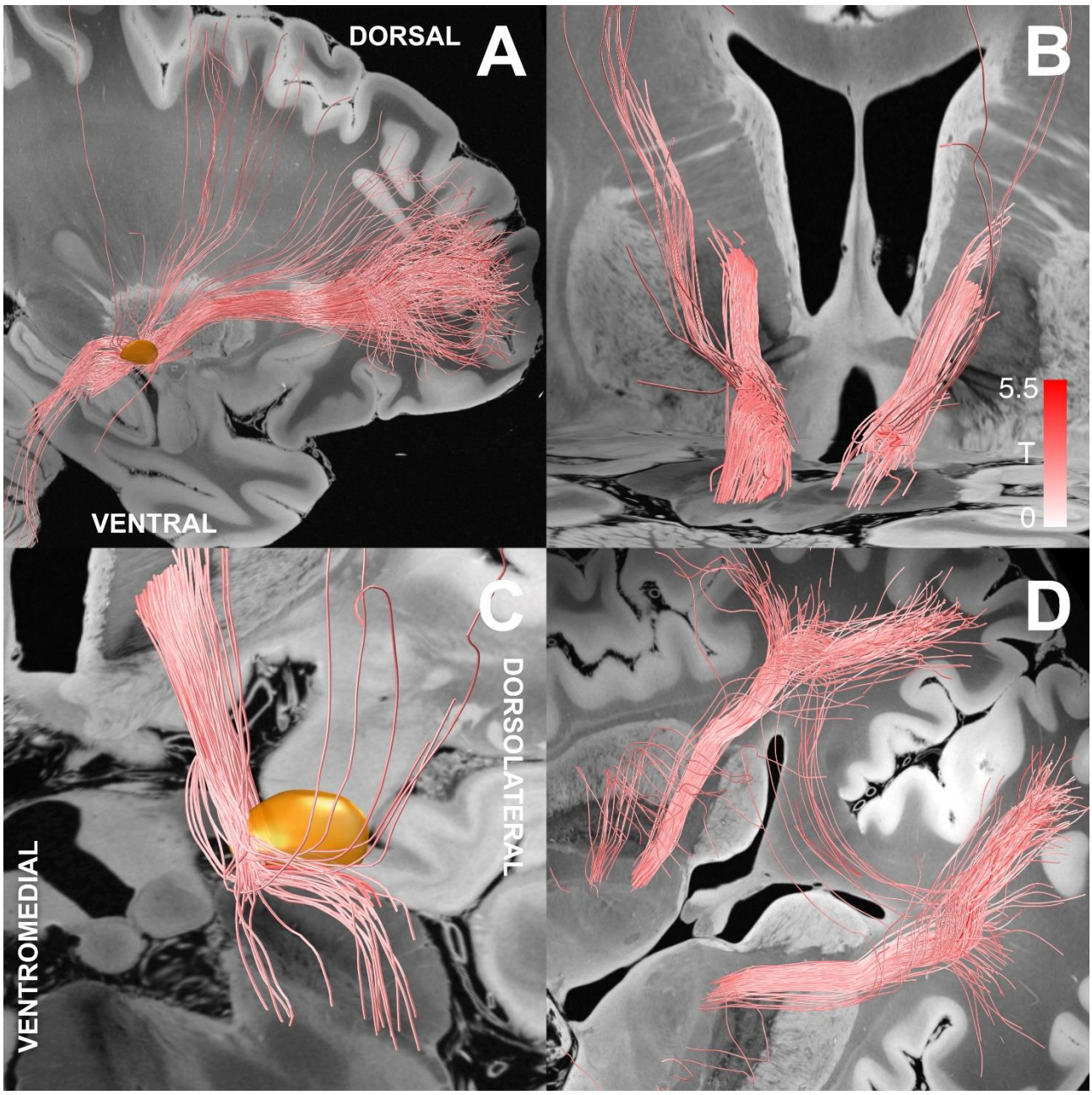


**Figure S3.** Positively predictive fiber tracts that were commonly discriminative in both ALIC- and STN-cohorts shown from multiple angles to further characterize them, anatomically. A) Sagittal overview with STN in orange. B) Trajectory within the internal capsule while it passes putamen and caudate. C) Close-up showing the tracts course within and below the anterior STN. D) Oblique view of the axial aspect after entering the anterior limb of the internal capsule coming in from ventrally.

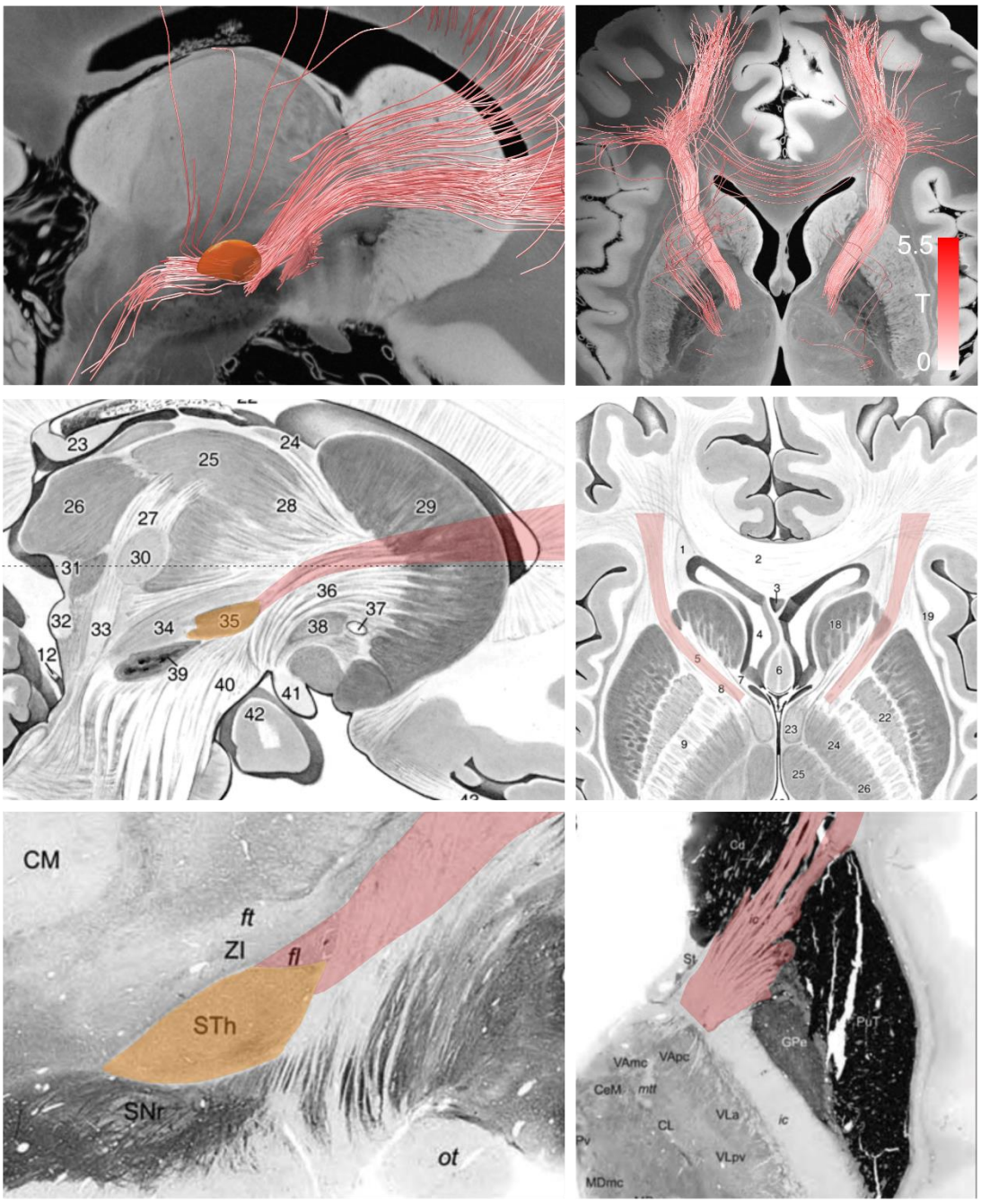


**Figure S4.** Direct synopsis of the tract target (top row) with anatomical white-matter textbook definitions. Mid-row shows data adapted with permission from [39], bottom row from [88].

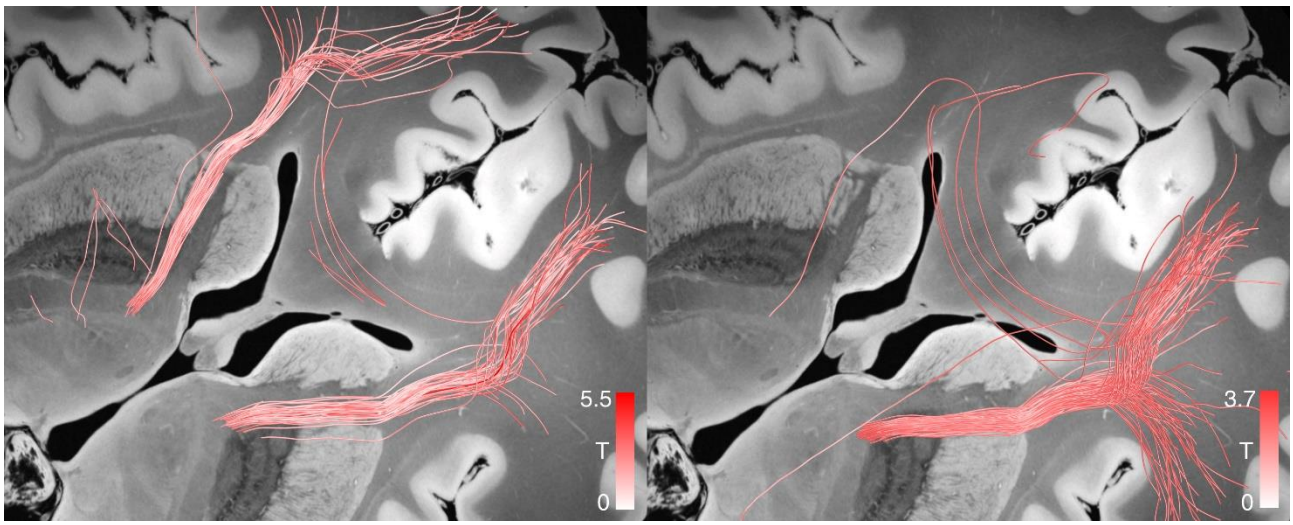


**Figure S5.** Right lateralization of the predictive tract in the training/cross-prediction sample (Grenoble and Cologne; N = 36) as well as the test sample (London; N = 6). As reported in prior studies, the right hemisphere may play a more crucial role in alleviating treatment response of DBS for OCD.